22-357

Behavior of Concrete Bridge-Deck Slabs Reinforced with Basalt Fiber-Reinforced Polymer and Steel Bars

by Yahia M. S. Ali, Xin Wang, Shui Liu, and Zhishen Wu

Recently, hybrid reinforcement by combining steel with fiber-reinforced polymer (FRP) bars has emerged as a new system in reinforced concrete (RC) constructions. This reinforcement system can effectively overcome the ductility and serviceability challenges of FRP-RC structures. A total of 11 full-scale bridge-deck slabs were constructed and tested. The test parameters were reinforcement type, ratio, arrangement, and slab thickness. Moreover, a comparison between the experimental and predicted deflections from design provisions was carried out to verify the efficiency of the models for hybrid RC sections. Based on test results, hybrid RC slabs exhibited ductility leading to an ample warning before failure rather than brittle shear failure observed for FRP-RC slabs. In addition, hybrid RC slabs displayed good stiffness, serviceability, and load-carrying capacity. Furthermore, test results give an average bond-dependent coefficient, k_b, *of 1.27, close to the 1.2 recommended by ACI CODE-440.11-22. In addition, some modifications were proposed to shear equations available in different design codes to be valid for hybrid RC members without shear reinforcement.*

Keywords: basalt fiber-reinforced polymer (BFRP) bar; concrete bridge; hybrid reinforcement; shear behavior.

INTRODUCTION

Bridge-deck slabs are the most critical infrastructure exposed to harsh environments (deicing salts, humidity, freezing-and-thawing cycles, and chlorides) that make these structures very susceptible to corrosion of steel reinforcement. The associated deterioration can accelerate such failure or reduce the expected life span of the structure. Within the past two decades, the most effective way to diminish maintenance costs and extend the life span of structures has been to use fiber-reinforced polymer (FRP) composites as an alternative to traditional steel reinforcement in structural components, especially where steel corrosion is a major concern. In addition to corrosion resistance, FRP composites have many characteristics over steel reinforcement, such as a high strength-to-weight ratio, excellent fatigue resistance, and nonmagnetic and nonconductive nature, which can be used in harsh environments for civil structures. Unfortunately, FRP composites have some drawbacks: a low elastic modulus compared to steel (E_f/E_s = approximately 0.25) and linear-elastic behavior up to failure without presenting any yielding plateau, which resulted in the brittle collapse of the member (Goldston et al. 2016). Many investigations have been performed to study the overall performance of concrete members reinforced with FRP bars. FRP-reinforced slabs had larger deflections and wider crack widths and depths compared to steel-reinforced slabs (Michaluk et al. 1998; Ferrier et al. 2015). Therefore, serviceability criteria often govern the design of FRP-reinforced concrete (RC) members in most instances. ACI 440.1R-15 (ACI Committee 440 2015) and CSA S806-12 (2017) permit using glass FRP (GFRP), carbon FRP (CFRP), and aramid FRP (AFRP) bars in concrete constructions.

Basalt fibers have been introduced as a promising addition to the current types of FRPs. Basalt FRP (BFRP) bars have relatively greater strength and modulus, comparable costs, and higher chemical resistance than GFRP bars (Wu et al. 2015). Thus, using BFRP bars with a relatively high elastic modulus, compared to GFRP bars, would significantly decrease the amount of reinforcement required and reduce the crack width (Elgabbas et al. 2016). Moreover, BFRP-RC beams exhibited acceptable deformability when investigated in flexure and shear (Duic et al. 2018).

LITERATURE REVIEW

In FRP-RC members, deeper cracks reduce the contribution of uncracked concrete to the shear stress due to the lower concrete depth in compression. Moreover, in the transverse direction, FRP bars have lower strength and stiffness, which led to wider cracks and lower aggregate interlock and dowel action supplement to the tensile reinforcement compared to that of an equivalent steel area (El-Sayed et al. 2006a). Finally, the total shear strength of FRP-RC members is lower than that of steel-RC members. However, traditional stirrups are not feasible for constructing slab bridges; consequently, the mode of failure may be dominated by shear (Abdul-Salam et al. 2016). Slabs reinforced with GFRP or CFRP bars failed in diagonal tension failure, while the steel-reinforced slabs failed in ductile flexure mode by steel yielding followed by concrete crushing (El-Salakawy and Benmokrane 2004). In addition, increasing the reinforcement ratio significantly improved the shear strength and the post-cracking stiffness (El-Sayed et al. 2005; Matta et al. 2013). Thus, the reinforcement type and its axial stiffness can be confirmed to have a pronounced effect on the shear strength of the RC sections.

Gradual failure can be attained by using both FRP and steel reinforcements. Therefore, steel reinforcement improves the ductility by the yielding of steel reinforcement and enhances serviceability by decreasing the deflection and crack width, while FRP reinforcement maintains the load-carrying

ACI Structural Journal, V. 120, No. 5, September 2023.
MS No. S-2022-357.R1, doi: 10.14359/51738840, received April 27, 2023, and reviewed under Institute publication policies. Pertinent discussion including author's closure, if any, will be published ten months from this journal's date if the discussion is received within four months of the paper's print publication.

capacity even after the yielding of steel bars (Qin et al. 2017). In addition, hybrid reinforcement resulted in lower crack spacing and smaller widths (Aiello and Ombres 2002). From a durability approach, the FRP bars were placed on the outer layer to attack the harsh conditions, and the steel bars were placed on the inner layer with an adequate cover to keep them away from corrosion. However, placing steel and FRP bars in one layer presented better flexural strength than placing FRP bars in the outer layer and steel bars in the inner layer (Yinghao and Yong 2013). It is found that the effective reinforcement ratio has a major impact on the flexural capacity compared with axial stiffness between GFRP and steel bars (R_f) (Qu et al. 2009). GFRP-steel RC beams showed slightly lower flexural capacity than steel-RC beams. However, the deflection and maximum crack width were large in beams reinforced with steel reinforcement at service load (Ruan et al. 2020). Furthermore, the ductility of hybrid reinforced beams can satisfy the specifications of serviceability limits by adequately regulating the reinforcement ratio and the A_f/A_s value (Ge et al. 2015). In addition, the maximum load and moment for serviceability increased with the GFRP-to-steel ratio. At the ultimate stage, the deflection obviously increases and provides a good pre-failure warning (Xingyu et al. 2020). Applying the principle of equal stiffness, the overall performance of the hybrid RC beams was superior when $A_s/A_f \leq 1.0$; however, it declined intensely when $A_s/A_f > 1.0$ (Wang et al. 2022).

An alternative method was proposed by (Nanni et al. 1994) to protect the steel bar from corrosion by covering the steel core with a braided and epoxy-coated aramid or vinylon fiber FRP skin. Wu et al. (2012) developed a new kind of hybrid bar, a steel-FRP composite bar (SFCB) that combines a ribbed steel bar inside and a longitudinal FRP outside in a pultrusion process. The SFCB was created by modifying FRP pultrusion technology. The benefits of an SFCB are: 1) the pultrusion process and the ribbed inner steel bar ensure good interface properties and optimal use of each material; 2) excellent durability with the outer FRP; 3) a high elastic modulus of the SFCB due to the contribution of steel at the initial stage; 4) noticeable post-yield modulus in the stress-strain relationship after the inner steel bar yields; and 5) high strength, good ductility, anti-erosion properties, and low cost (Wu et al. 2009).

Many studies investigated the behavior of concrete members reinforced with SFCBs: beams (Sun et al. 2012; Ge et al. 2020; Yang et al. 2020), slabs (Ali et al. 2023), and columns (Sun et al. 2011; Ibrahim et al. 2017). It is found that beams reinforced with SFCBs displayed stable post-yield stiffness after the inner steel bar yielded. Although yielding the same ratio between steel and FRP, the ultimate capacity of the beam reinforced with BFRP and steel bars showed only 72% of that reinforced with SFCBs. This is attributed to the high bond stress in the hybrid beam, which led to the early slip of BFRP bars (Sun et al. 2012). Moreover, SFCB-RC beams showed enhanced stiffness, reduced crack width, and higher moment capacity than their counterparts reinforced with FRP bars (Ge et al. 2020). Using SFCB and BFRP bars as the main reinforcement exhibited better serviceability and ductility compared to conventional hybrid RC beams (Yang et al. 2020).

To the authors' best knowledge, no research has been carried out studying the performance of concrete bridge-deck slabs reinforced with hybrid bars. Therefore, it is necessary to comprehend how these types of structures behave and later to allow and incorporate this concept into bridge design codes and specifications. Based on the authors' previous studies of this bridge deck (Ali et al. 2023), the structural behavior of the hybrid RC bridge-deck slabs without shear reinforcement was studied considering the most effective parameters that affect the deck slab performance.

RESEARCH SIGNIFICANCE

The novelty of this paper is to shed light on the structural behavior of the BFRP/steel-RC deck slabs without shear reinforcement. The slabs' performance was evaluated in terms of cracks propagations and failure modes, load-deflection response, reinforcement and concrete strains, stiffness, ductility taking into consideration the effects of reinforcement type and ratio, A_f/A_s ratio, and slab thickness. The experimental test results were used to verify the accuracy of existing models to predict the load-deflection response and to evaluate the bond-dependent coefficients, k_b, of the ribbed BFRP bars. In addition, some modifications were proposed to different code equations to predict the shear strength of hybrid RC slabs with reasonable accuracy.

EXPERIMENTAL INVESTIGATION

Design concept

The sum of the FRP reinforcement ratio, ρ_f, and steel reinforcement ratio, ρ_s, cannot be applied to directly express the reinforcement ratio of hybrid sections owing to the variations in mechanical properties between steel and FRP bars. Two types of reinforcement ratios, $\rho_{sf,s}$ and $\rho_{sf,f}$, were defined to account for combinations of the elastic modulus and strength, respectively (Pang et al. 2016). The corresponding balanced reinforcement ratios can be calculated as: $\rho_{s,b}$ is the reinforcement ratio when concrete crushing and steel yielding happen synchronously; and $\rho_{f,b}$ is the reinforcement ratio when concrete crushing and FRP bar rupturing occur simultaneously as follows

$$\rho_{sf,s} = \rho_s + \frac{E_f}{E_s}\rho_f \tag{1}$$

$$\rho_{sf,f} = \frac{f_y}{f_{fu}}\rho_s + \rho_f \tag{2}$$

$$\rho_{s,b} = \alpha_1\beta_1\frac{f_c'}{f_y}\frac{\varepsilon_{cu}}{\varepsilon_{cu}+\varepsilon_y} \tag{3}$$

$$\rho_{f,b} = \alpha_1\beta_1\frac{f_c'}{f_{fu}}\frac{\varepsilon_{cu}}{\varepsilon_{cu}+\varepsilon_f} \tag{4}$$

Hybrid FRP-steel slabs were designed in which $\rho_{sf,s} \leq \rho_{s,b}$ and $\rho_{sf,f} \geq \rho_{f,b}$. Therefore, the designed failure mode can be defined as follows: firstly, the steel bars yield; subsequently, the concrete is crushed in compression; and lastly, the slab fails. This failure would provide sufficient warning before slab failure can be attained.

Material properties

The deck slab specimens are fabricated using normal-weight ready mixed concrete to cast all the slabs on the same day. The concrete mixture design proportions per cubic meter are 169 L of water, 452 kg of cement, 639 kg of sand, 1088 kg of aggregate, and an air content of 5 to 6% to achieve a slump of 150 ± 30 mm. The average compressive strength was evaluated by testing three standard 150 mm concrete cubes after 28 days of curing. The concrete cubes yielded an average compressive strength of 52 ± 1.3 MPa. It is worth mentioning that the cylinder compressive strength of concrete, f_c', was calculated based on ACI codes, whereas $f_c' = 0.8f_{cu}$. The reinforcing bars used in this paper included ribbed steel bars, BFRP bars, and SFCBs, as shown in Fig. 1. BFRP bars are made of basalt fibers and epoxy resin, and basalt fiber content by weight is 70% according to the manufacturer. For SFCB production, 10 mm diameter inner ribbed steel bars were used and wrapped with basalt fibers that consisted of BFRP combined with a vinyl ester resin. Axial tensile tests were conducted to evaluate the mechanical properties of the different reinforcing bars according to ASTM D7205/D7205M (2016), as applicable. The results of the average three specimens of reinforcing bars are reported in Table 1 and shown in Fig. 2.

Fig. 1—Configuration of BFRP and SFCB reinforcing bars: (a) geometry of BFRP and SFCB bars; and (b) cross sections.

Test specimens

Eleven large-scale RC slabs with a total length (L_t) of 2900 mm and a width (b) of 1000 mm were used. The boundaries of the slabs were delineated considering the contraflexural lines. Moreover, these dimensions are the most popular size of the bridge-deck slabs for girder-type in North America (El-Salakawy et al. 2003; El-Salakawy and Benmokrane 2004). Nine slabs had a depth (h) of 200 mm (according to the requirements of CSA S6 [2019]), one slab had a depth of 250 mm, and the last one had a depth of 120 mm. The investigated parameters were the reinforcement type, effective reinforcement stiffness $\rho_{sf,s}$, the ratio between the area of FRP and steel bars A_f/A_s, reinforcement arrangement, and slab thickness. All slabs have the same steel reinforcement in all directions, 12 mm with a spacing of 225 mm, except the bottom longitudinal reinforcement. The clear concrete covers were 50 mm and 25 mm for the top and bottom reinforcement, respectively. The slab specimens were identified according to the amount and type of longitudinal reinforcement (XB or XBXS), where the letters X, B, and S indicate the number of bars, BFRP reinforcing bar, and steel reinforcing bar, respectively.

The test program was categorized into four groups based on the test parameters studied. Group A (reference group) consists of two slabs (8B and 5B3S) studying the effect of reinforcement type. In Group B, slabs (5B7S, 6B7S, and 10B6S) investigate the influence of increasing the effective reinforcement stiffness, $\rho_{sf,f}$, compared to Group A. It is worth noting that the slabs in this group were designed with similar $\rho_{sf,s}$ to study the impact of the A_f/A_s ratio. Group C includes slabs (5B5S, 5S5B, and 5B5S-S) that vary in reinforcement arrangement, where S (the last letter in Slab 5B5S-S) represents that the reinforcement is arranged in a single layer. Regarding Slab 5S5B, which placed steel bars at the outer layer, it is not efficient from the durability point of view; this system is examined only to evaluate the influence of the reinforcement arrangement on the structural performance

Table 1—Properties of reinforcing bars

Bar type	d, mm	E_I, GPa	f_y, MPa	E_{II}, GPa	f_u, MPa	ε_u, %
Steel	10	200	420	—	632	3.30
	12	200	452	—	667	3.16
	16	200	494	—	688	3.50
BFRP	15.6	55 ± 0.60	—	—	1163 ± 27.3	2.12 ± 0.12
SFCB	15.5	105 ± 2.4	263 ± 4.7	32 ± 3.2	756 ± 16.2	3.71 ± 0.16

Note: 1 mm = 0.0394 in.; 1 MPa = 145 psi; 1 GPa = 0.145 ksi.

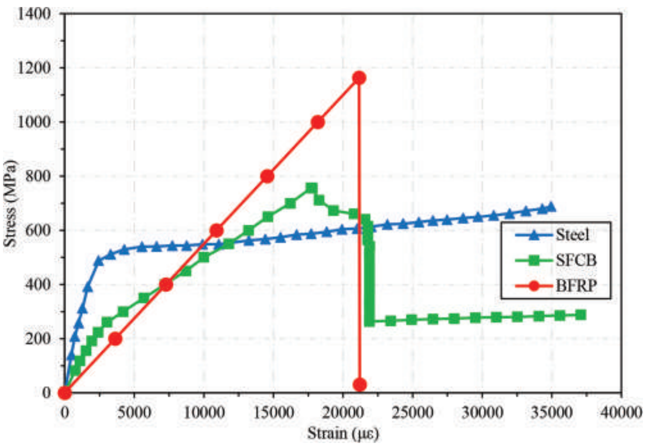

Fig. 2—Stress-strain relationships of reinforcements.

of the hybrid deck slabs. The last group comprised three slabs (9SFCB-200, 9SFCB-250, and 9SFCB-120) with three different thicknesses (200, 250, and 120 mm) to study the effect of different slab thicknesses. Table 2 summarizes the details of the slabs. Figure 3 shows the cross sections of all deck slabs.

Test program and instrumentation

The slabs were tested under four-point bending loading up to failure. Figure 4 provides the test setup and schematic diagram of the slabs. A steel spreader beam was used to transform the two concentrated loads 900 mm apart, yielding a shear span (*a*) of 900 mm on both sides with a clear span length (*L*) of 2700 mm. Two half cylinders with 100 mm diameters were used for loading; however, two full cylinders were used to support the slab specimens, as shown in Fig. 4. The load was applied with displacement control at a constant rate of 0.6 mm/min by the hydraulic jack of 500 kN capacity to measure the applied loads with a displacement sensor to measure the corresponding deflection. The load gradient was established at 5 kN up to an applied load of 100 kN to detect crack widths. After the applied load reached 100 kN, the load gradient was increased to 10 kN until the failure of the slab. Three linear variable differential transformers (LVDTs) were positioned at the bottom midspan and the two loading points of each slab, and two LVDTs were installed at the supports to offset their settlements. Five electrical strain gauges were attached to the slab surface to measure the concrete strain along the depth of the slab, and four strain gauges were also attached to the surface of the tensile reinforcement. The applied loads, deflections, and strain readings at a frequency of 10 Hz were automatically recorded using a data acquisition system. The crack width was measured using a handheld readout microscope with a magnification factor of 40× with an accuracy of 0.01 mm.

EXPERIMENTAL RESULTS AND DISCUSSION

Crack patterns and propagation

Figure 5 shows the crack distribution of the tested deck slabs upon failure. The first crack was initiated in the pure bending moment zone. Generally, the cracking load was recorded at a similar load level for slabs of the same thickness, while increasing the slab thickness increased the cracking load, as listed in Table 3. As the load increased, more flexural cracks began to develop below or between the point loads. With further loading, flexural-shear and shear cracks appeared and spread in the shear spans, demonstrating the shear stresses in the shear span. Once the steel yielded, the number of cracks increased and propagated, accompanied by the widening of the existing cracks.

Slab 8B showed a larger number of shear cracks, and the crack length propagated quickly due to the low stiffness modulus of the BFRP bar. In addition, Slab 8B yielded higher crack spacing, more severe cracking, and a lower number of cracks than Slab 5B3S, thus tending to suggest substituting BFRP bars with steel bars to improve the axial stiffness of the slab. Increasing the reinforcement ratio increases the number of major and minor cracks, improves the crack distribution length, and reduces the average minor and major crack spacing. This result is clarified by better bond strength as the number of longitudinal bars increases (Nguyen et al. 2020). Moreover, Slab 5B7S displayed low average crack spacing at the same load level compared to Slab 10B6S. The same phenomenon was reported by (Ge et al. 2015); the average crack spacing diminishes with the reduction of A_f/A_s.

Table 2—Details of tested slabs

Group No.	Slab	A_f/A_s	$\rho_{sf,s}$ %	$\rho_{sf,f}$%	$\rho_{sf,s}/\rho_{s,b}$	$\rho_{sf,f}/\rho_{f,b}$
A	8B	—	0.25	0.89	0.09	3.14
	5B3S	1.58	0.59	0.75	0.20	2.65
B	5B7S	0.68	1.18	1.00	0.40	3.53
	6B7S	0.81	1.19	1.12	0.41	3.95
	10B6S	1.58	1.18	1.48	0.40	5.22
C	5B5S	0.95	0.88	0.93	0.30	3.28
	5S5B		0.79	1.00	0.27	3.53
	5B5S-S		0.76	0.88	0.26	3.11
D	9SFCB-200	1.40	0.59	0.82	0.20	2.05
	9SCFB-250		0.46	0.64	0.15	1.60
	9SCFB-120		1.14	1.59	0.38	3.98

Modes of failure

The combined effect of high shear force and bending moment leads to a spatially high-stress area; hence, failure occurs in the shear span. Four different failure modes were observed in the experimental tests and are listed in Table 3.

Mode I: Diagonal tension failure (DTF)—This mode was observed only for Slab 8B reinforced with BFRP bars owing to the low stiffness of BFRP bars, as shown in Fig. 5. At a high load level, the shear cracks continued to widen due to the absence of shear reinforcement until failure occurred. The diagonal shear crack occurred at 100 mm far from the support, making it approximately 42 degrees with the horizontal, then extended toward the loading point and widened and propagated, leading to slab collapse. Moreover, the failure was accompanied by local bending of steel bars in the compression zone keeping the slab intact as one part, as shown in Fig. 6. This phenomenon led to improved ductility and integrity of the slab. In contrast, a previous

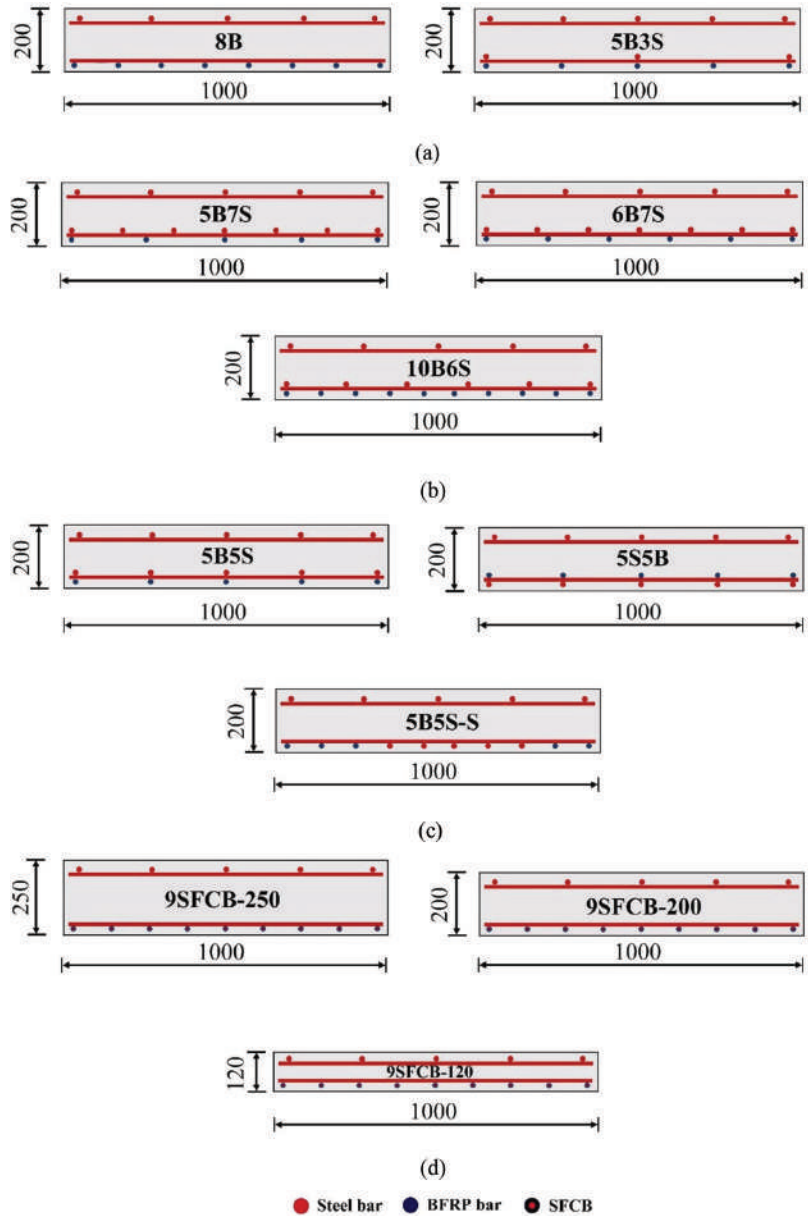

Fig. 3—Reinforcement details of tested deck slabs: (a) Group A; (b) Group B; (c) Group C; and (d) Group D. (Note: Dimensions in mm; 1 mm = 0.0394 in.)

study observed that using FRP bars in the compression zone resulted in the shearing off of FRP bars, and the slabs were divided into two parts (Abdul-Salam et al. 2016).

Mode II: Flexural-shear failure (FSF)—This mode was observed for Slabs 5B3S, 5B5S, 5S5B, and 9SFCB-200, which initiated as a flexural crack closer to the loading point and then propagated inclining upward to the loading point. As shown in Fig. 5, the failure was gradual, and the slabs displayed some ductility before reaching the ultimate load, rather than the brittle shear failure observed in Slab 8B. This may be attributed to the higher load levels reached, which confirms the enhancement of the shear resistance by the improved dowel action of the double-layer reinforcement (Yoo et al. 2016).

Mode III: Shear-compression failure (SCF)—In this mode, the compression zone in the slab was reduced by the inclined flexure-shear cracks; thus, the concrete was crushed in Slabs 6B7S, 10B6S, and 5B5S-S, as shown in Fig. 5. The main crack that makes the failure for these slabs has an inclined degree of 55 to 68 degrees. Additionally, the failure was accompanied by concrete-cover spalling on the tension side without FRP bars shearing off, and the slab maintained its integrity even after failure, which can be attributed to the high reinforcement ratio and A_f/A_s in these slabs. Accordingly, a minimum amount of steel reinforcement with a reasonable value of A_f/A_s is recommended to ensure ductility and prevent the devastating failure of concrete bridge-deck slabs.

Regarding the arrangement of reinforcement, Slab 5B5S-S, with reinforcement arranged in a single layer, exhibited severe failure compared with its counterparts arranged in a double layer owing to deteriorated bond performance caused by the small spacing of the reinforcement (Yang et al. 2020). Minor differences were noted in the distribution and shape of the flexural cracks for all tested slabs. However, the slab failure mechanism changes between the BFRP-RC slab and

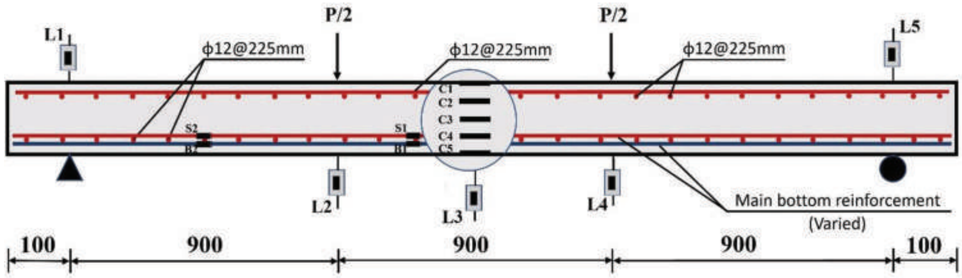

(a)

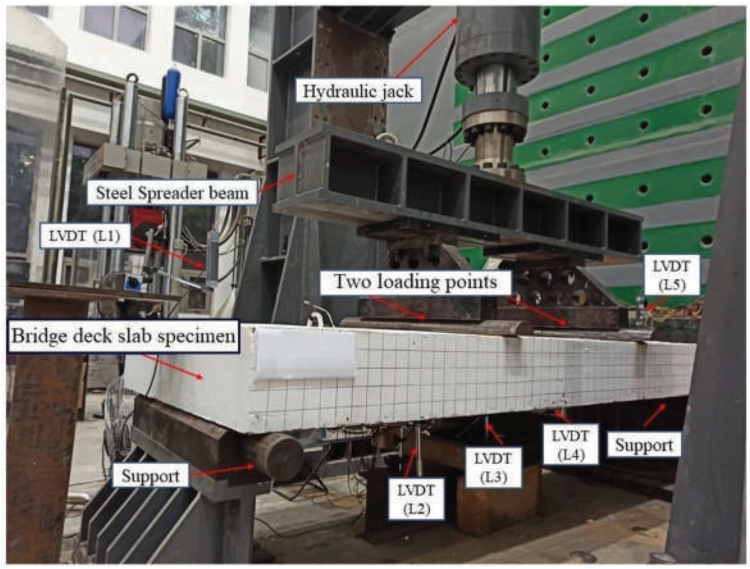

(b)

Fig. 4—Test setup: (a) schematic drawing; and (b) slab specimen ready for testing. (Note: Dimensions in mm; 1 mm = 0.0394 in.)

hybrid RC slabs could be due to the difference in the shear-crack location. The shear crack in Slab 8B initiated closer to the support due to the diagonal tension stresses, resulting in a crack closer to the support (100 mm). In contrast, Slab 5B3S experienced no significant shear cracks, which moved the crack location closer to the loading point (300 mm). It can be related to the contribution of arch action, which was dependent on the critical shear-crack location. The crack was far from the support in hybrid slabs, allowing the arch action to contribute more.

A discussion of flexural analysis was presented (refer to the Appendix*), demonstrating that the hybrid RC slabs reached their flexural capacities before failure. Therefore, this failure is considered a combination of flexural and shear failure.

Mode IV: Flexural failure (FF)—This mode was observed for Slabs 5B7S, 9SFCB-250, and 9SFCB-120 by steel yielding where the main crack was approximately under the point load. These slabs did not display any bond-splitting cracks, which shifted the crack location closer to the loading point. Generally, using hybrid reinforcement to reinforce the deck slabs, either separate reinforcing bars or SFCBs, could achieve some plastic deformations of concrete before total failure; thus, this type of section is admissible in the design of hybrid RC members without shear reinforcement.

Strain distribution

Figure 7 shows the strain distribution of concrete along the cross-section height at various loading stages. The average concrete strain along the cross-section height is almost linear and proportional to the distance from the neutral axis, reflecting that the assumption of the plane cross section is valid for hybrid RC slabs, as shown in Fig. 7. The depth of the neutral axis of FRP-reinforced deck slab 8B was smaller than the depth of the neutral axis of hybrid reinforced deck slab 5B3S, indicating the influence of the modulus of the steel bars when added to the slab reinforcement.

Ultimate capacity

The ultimate capacity for all tested slabs is listed in Table 3. The test results revealed that hybrid slab 5B3S showed a slight increase of 6% in the ultimate capacity compared with Slab 8B reinforced with pure BFRP bars. This is attributed to the amount of BFRP bars in Slab 5B3S being less than that of Slab 8B, whereas BFRP bars are responsible for carrying the additional load after the steel yielded. In addition, the ultimate capacity increased, as did the reinforcement ratio (Tureyen and Frosch 2002). For example, Slab 6B7S showed an increase in the ultimate capacity of 39% compared to control slab 5B3S. This is due to the function

*The Appendix is available at **www.concrete.org/publications** in PDF format, appended to the online version of the published paper. It is also available in hard copy from ACI headquarters for a fee equal to the cost of reproduction plus handling at the time of the request.

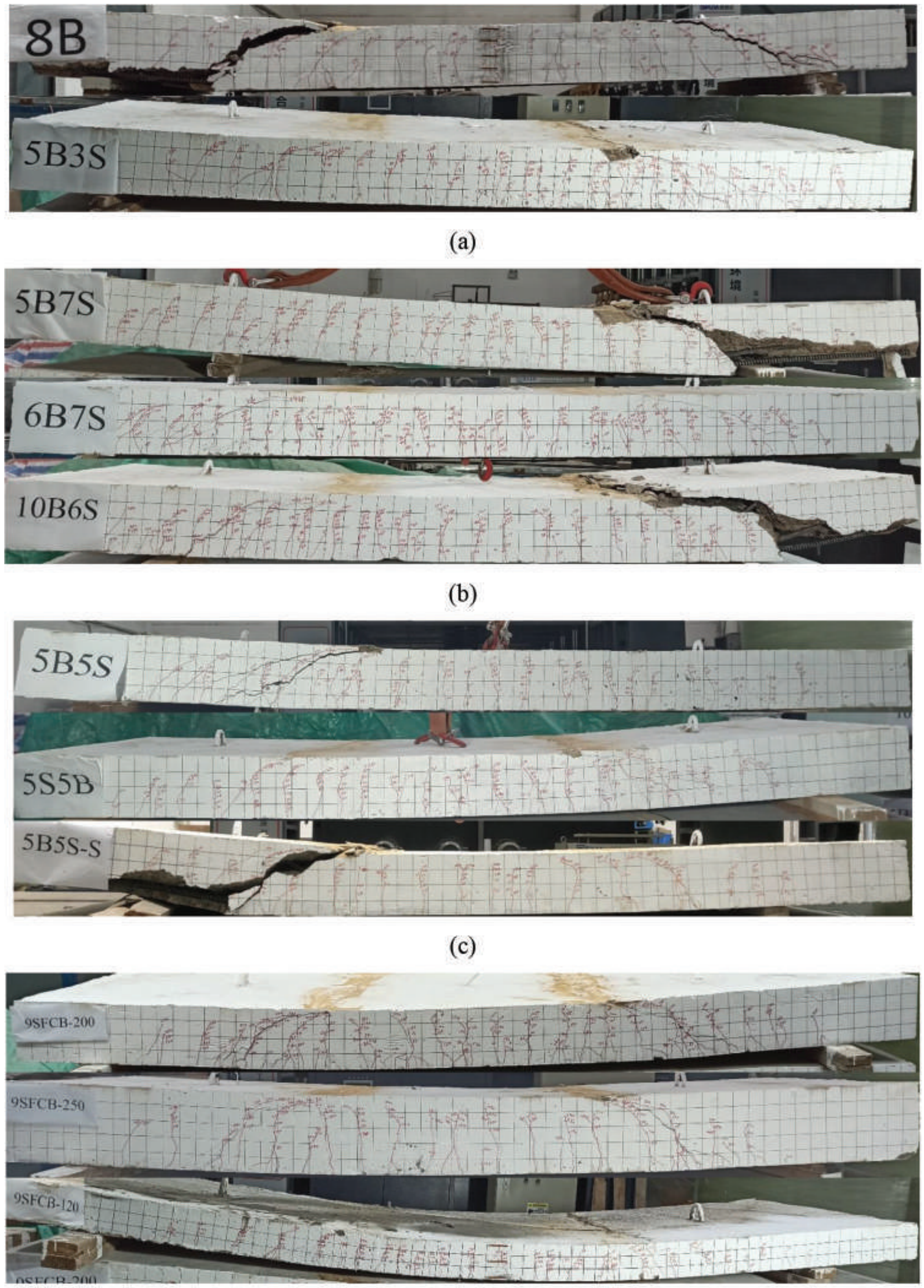

Fig. 5—Crack patterns and failure modes of tested slabs: (a) Group A; (b) Group B; (c) Group C; and (d) Group D.

of the longitudinal reinforcement in decreasing the opening and propagation of cracks resulting in smaller crack width, which increases the uncracked concrete depth and improves the aggregate interlock across the cracks. Moreover, Slab 10B6S contains the highest FRP-to-steel content (A_f/A_s = 1.58) and showed an improvement in ultimate capacity by 13% compared with Slab 5B7S (A_f/A_s = 0.68).

The reinforcement arrangement affects the ultimate capacity because Slab 5B5S-S, reinforced in a single layer, exhibited higher ultimate capacity than slabs arranged in a double layer. The ultimate capacity of Slab 5B5S-S is approximately 1.22 and 1.18 times the ultimate capacity of Slabs 5B5S and 5S5B, respectively. From the mechanical point of view, placing the BFRP and steel bars at the outer layer is more effective than placing the BFRP bars at the outer layer. Experimental results from Slab 9SFCB-250 showed that shear capacity could be enhanced with increasing slab stiffness compared to Slab 9SFCB-200. The ultimate shear capacity of Slab 9SFCB-200 was 292 kN, while Slab 9SFCB-250 failed at 359 kN, that is, a 23% improvement. Increasing the slab thickness increases the surface area that resists the shear stresses, yielding higher shear capacity.

Load-deflection relationship

Figure 8 shows the load-midspan deflection curves for the tested deck slabs. All slabs showed a steep linear behavior at the pre-cracking stage with low deflection values. In the post-cracking stage, slab stiffness was significantly degraded

Table 3—Test results of tested slabs

Group	Slab	Δ_{cr}, mm	Δ_y, mm	Δ_u, mm	P_{cr}, kN	P_y, kN	P_u, kN	M_{exp}/M_{pred}	Failure mode
A	8B	2.3	—	63	36	—	295	0.80	DTF
	5B3S	1.7	19.1	78	41	179	314	1.43	FSF
B	5B7S	1.2	22.3	67	42	260	414	1.56	FF
	6B7S	2.0	20.1	49	46	251	437	1.59	SCF
	10B6S	1.9	20.3	45	47	294	470	1.62	SCF
C	5B5S	2.3	20.6	68	43	190	325	1.42	FSF
	5S5B	2.3	18.4	73	38	190	335	1.34	FSF
	5B5S-S	3.7	16.5	58	49	211	396	1.51	SCF
D	9SFCB-200	1.5	13.3	77	34	146	292	1.23	FSF
	9SFCB-250	3.1	13.2	65	99	212	359	1.22	FF
	9SFCB-120	8.8	21.9	144	26	69	147	2.18	FF
Average*			—	—	—	—	—	1.51	—
Standard deviation*			—	—	—	—	—	0.26	—
Coefficient of variation*, %			—	—	—	—	—	17	—

*These characteristics were calculated only for hybrid RC deck slabs; DTF is diagonal tension failure; FSF is flexural-shear failure; FF is flexural failure; SCF is shear-compression failure.

Note: 1 mm = 0.0394 in; 1 kN = 0.225 kip.

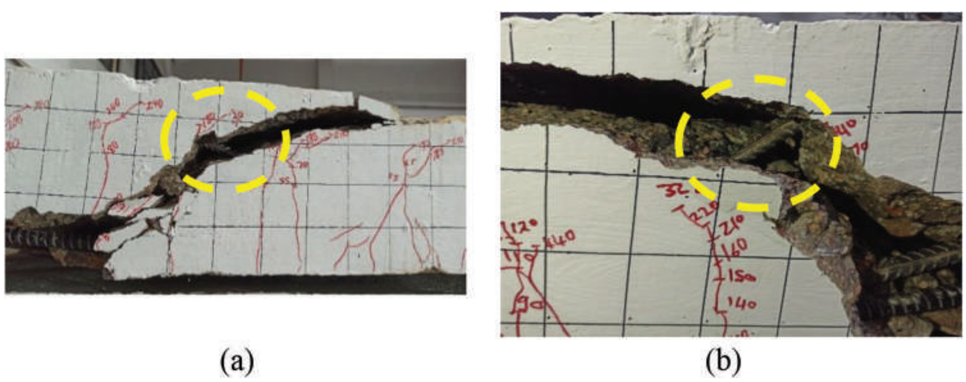

Fig. 6—Bending of steel bars in compression zone: (a) 8B; and (b) 10B6S.

due to flexural cracks, which reduced the moment of inertia. Slab 8B exhibited a bilinear load-midspan deflection curve and degraded faster than hybrid RC slabs due to the lower elastic modulus of the BFRP bars, as shown in Fig. 8(a). Conversely, hybrid RC slabs exhibited trilinear load-deflection curves owing to the presence of steel bars. As shown in Fig. 8, after steel yielded, a pronounced reduction in the slope of the load-deflection curves as the load increased to high levels means that steel reinforcement cannot resist any additional load, and only the BFRP reinforcement carried the load upon failure. In this stage, the deflection of hybrid deck slabs was lower than the deflection of Slab 8B, attributed to the efficiency of the BFRP bars restricting the excessive deflection even after steel yielding. Hence, using hybrid bars to reinforce the concrete bridge-deck slabs keeps the load growing with a reasonable deflection value.

In Group A, Slab 8B suffered a larger deflection than Slab 5B3S under the same load level, as shown in Fig. 8(a). This is attributed to the high elastic stiffness of steel bars compared to BFRP bars, which increased the rigidity of the hybrid slabs. At the yielding load of Slab 5B3S, the deflection decreased by 43% compared to Slab 8B. After steel yielding, a secondary stiffness was detected only for hybrid deck slabs. This observation proves the concept of the hybrid section that the significant role of FRP bars brightens after steel yielding. For Group B, increasing the reinforcement ratio increased the post-cracking stiffness, and hence decreased the deflection at similar load levels (El-Sayed et al. 2006b).

Regarding the A_f/A_s, there was a slight influence of the ratio of A_f/A_s on the stiffness after cracking. However, a significant enhancement in stiffness was noticed after steel yielding for Slab 5B7S in comparison to Slab 10B6S; thus, as A_f/A_s increases, the deflection decreases (Safan 2013). For example, at the load of 294 kN, the deflection of Slab 10B6S was 30% lower than the deflection of Slab 5B7S because the former had a high A_f/A_s, which enhanced the slab rigidity by restricting the excessive deflection after the steel yielded. The foregoing results proved the significant influence of the A_f/A_s on the post-elastic strength of bridge-deck slabs with sufficient deformability and stiffness.

Considering the reinforcement arrangement in Group C, both slabs reinforced in a double layer developed larger deflection than the slabs arranged in a single layer, as shown

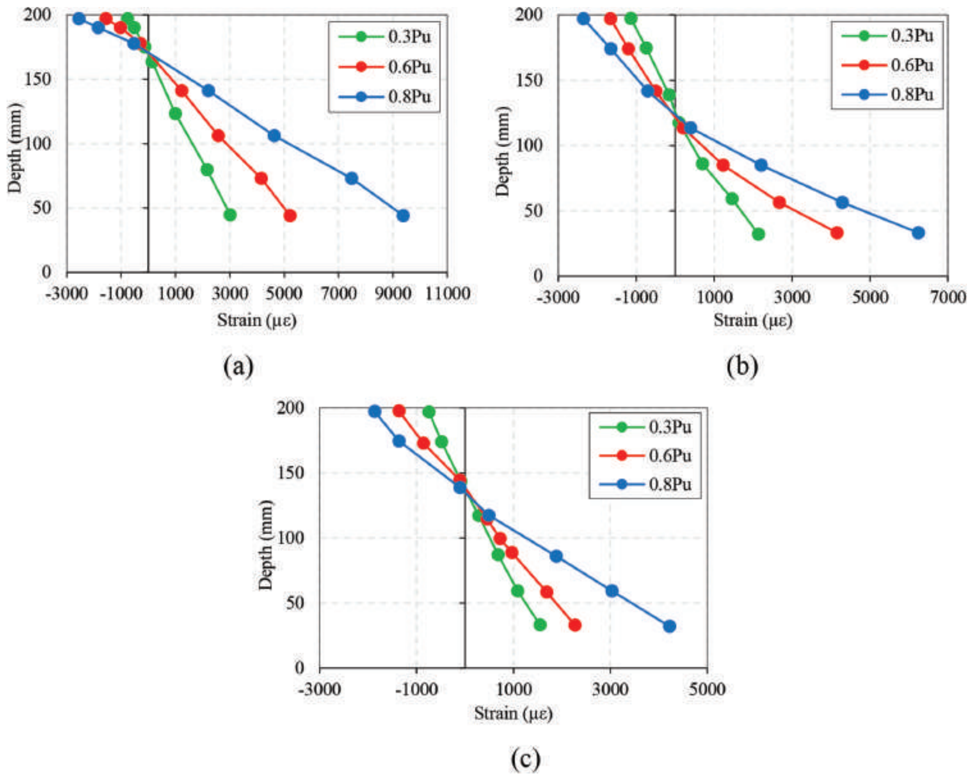

Fig. 7—Strain distribution of tested slabs: (a) 8B; (b) 5B3S; and (c) 10B6S. (Note: 1 mm = 0.039 in.)

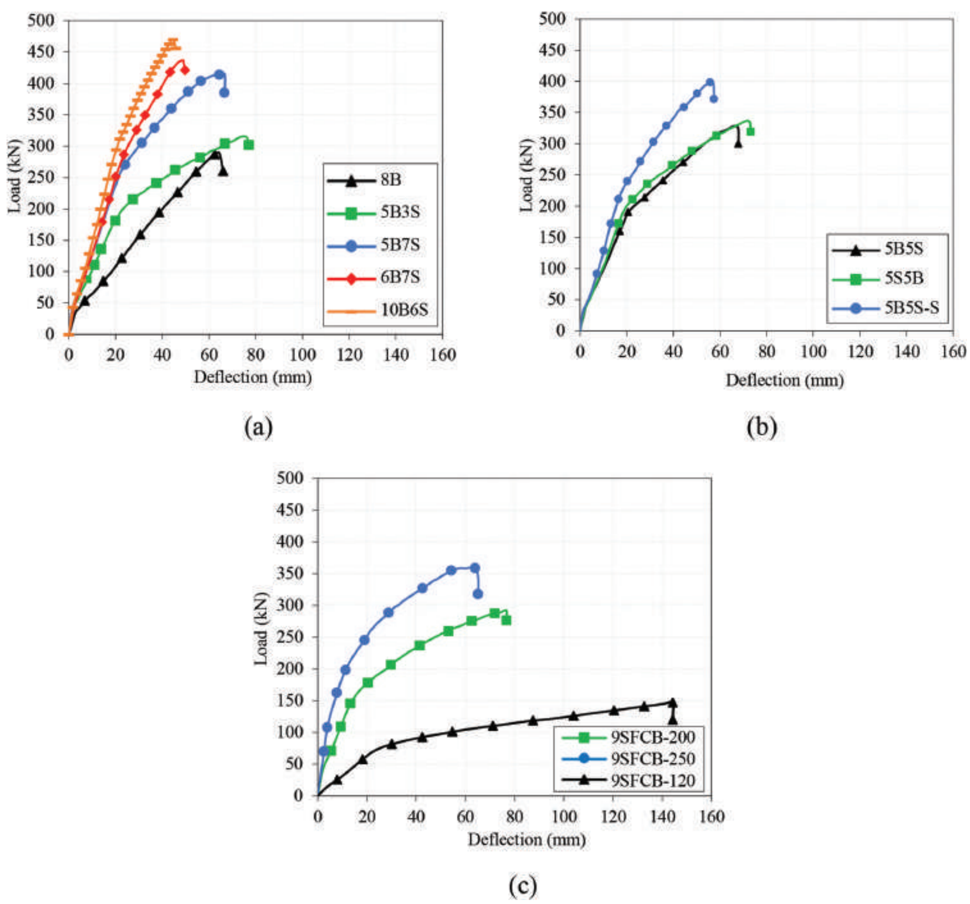

Fig. 8—Load-deflection relationships of tested slabs: (a) Groups A and B; (b) Group C; and (c) Group D. (Note: 1 kN = 0.225 kip; 1 mm = 0.0394 in.)

in Fig. 8(b). At a load of 200 kN (approximately the yielding load of this group), the deflections of Slabs 5B5S, 5S5B, and 5B5S-S were 23.9, 20.2, and 15.7 mm, respectively. This means that by increasing the depth of the steel bars layer, the stiffness degradation of the double-layer hybrid deck slab was faster than that of the single-layer hybrid deck slab (Yinghao and Yong 2013). The slab thickness had a clear effect on the stiffness of SFCB slabs, as shown in Fig. 8(c). An apparent reduction in the deflection was found when increasing the slab thickness from 120 mm to 200 and 250 mm while maintaining a constant reinforcement amount. This is due to increasing the moment of inertia of the slabs.

Stiffness

Based on the experimental test results, two stiffness factors were calculated to measure the stiffness of the tested deck slabs before and after yielding: the initial equivalent stiffness, K_I, and secondary stiffness, K_{II}, respectively (Sun et al. 2019).

$$K_I = \frac{P_y}{\Delta_y} \tag{5}$$

$$K_{II} = \frac{P_u - P_y}{\Delta_u - \Delta_y} \tag{6}$$

The stiffness factors are listed in Table 4. The results showed that the slab stiffness tended to improve with increasing the effective reinforcement ratio, $\rho_{sf,f}$, due to the improvement in the axial stiffness of the deck slab. Thus, Slab 5B3S designed with a low $\rho_{sf,f}$ suffered from stiffness degradation after cracking. Increasing the reinforcement ratio from 0.59 to 1.19% in Slabs 5B3S and 10B6S increased the initial and secondary stiffness K_I and K_{II} by 54% and 218%, respectively. A slight influence of A_f/A_s on the initial stiffness, K_I, and a significant enhancement of 83% in the secondary stiffness, K_{II}, was observed for Slab 6B7S in comparison to Slab 5B7S. This indicated that the initial equivalent stiffness was affected by steel reinforcement rather than BFRP reinforcement due to the significant variation in the elastic modulus (Nguyen et al. 2020). In contrast, the secondary stiffness depended on BFRP reinforcement due to steel yielding, which could not bear any additional load. The post-yielding stiffness of hybrid RC slabs can lead to a smaller residual deformation during unloading.

Table 4—Stiffness and ductility of tested slabs

Group	Slab	K_I	K_{II}	J_{mod}
A	8B	—	—	4.2
	5B3S	9.44	2.28	7.5
B	5B7S	11.64	3.48	5.3
	6B7S	12.52	6.38	5.1
	10B6S	14.50	7.24	4.8
C	5B5S	9.23	2.86	5.7
	5S5B	10.32	2.63	6.2
	5B5S-S	12.80	4.52	6.5
D	9SFCB-200	10.96	2.31	7.5
	9SFCB-250	16.15	2.80	6.3
	9SFCB-120	3.13	1.13	6.0

Consequently, the equal stiffness design principle is recommended to realize a damage-controllable structure under earthquakes (Wu et al. 2009; Wang et al. 2022). For Group C, the secondary stiffness, K_{II}, did not show a big difference between the two slabs arranged in double layers. However, K_{II} for Slab 5B5S-S was higher than both Slabs 5B5S and 5S5B, which means that the stiffness degradation of the double-layer hybrid deck slab was faster than that of the single-layer hybrid deck slab (Yinghao and Yong 2013). Among all the tested slabs, Slab 9SFCB-250 showed the highest initial stiffness, 16.15 kN/mm, due to increasing the moment of inertia, hence improving the slab stiffness; on the other hand, Slab 9SFCB-120 showed the lowest one, 3.13 kN/mm.

Ductility

Ductility refers to the amount of inelastic deformation that can be undergone without losing load-carrying capacity before complete failure. This paper adopted the deformation-based approach to evaluate the ductility of hybrid reinforced deck slabs. The overall performance factor, J, was adopted by CSA S6:19, which combines the strength and deformability provided by Eq. (7).

$$J = \frac{\Psi_u M_u}{\Psi_s M_s} \tag{7}$$

The moment and curvature at the serviceability limit state are taken as the point when the maximum concrete compressive strain reaches a value of 0.001. CSA S6:19 states that the overall performance factor, J, should be at least 4.0 for rectangular sections. Equation (7) uses service moments, M_s, at a concrete strain of 0.001, as recommended by CSA S6:19, neglecting the yielding of steel bars. Therefore, a modified overall performance factor, J_{mod}, was suggested for hybrid reinforced beams taken as the ratio of the product of moment and curvature at the ultimate to the product of moment and curvature at the yielding of steel reinforcement, as given in Eq. (8) (El Refai et al. 2015). It should be mentioned that J_{mod} was used only for slabs reinforced with hybrid reinforcement.

$$J_{mod} = \frac{\Psi_u M_u}{\Psi_y M_y} \tag{8}$$

Table 4 shows the values of the modified overall performance factor, J_{mod}, of all tested deck slabs. The inclusion of steel bars in Slab 5B3S improved the J_{mod} by 79% compared to Slab 8B. Slabs with lower reinforcement ratios showed a higher performance due to the proportional decrease in the stiffness of the slabs with the decrease in the reinforcement ratio (Liu et al. 2022). Increasing the reinforcement ratio from 0.59 to 1.18% (Slabs 5B3S and 10B6S) reduced the J_{mod} from 7.5 to 4.8. This is attributed to the enhanced reinforcement axial stiffness; increasing the reinforcement

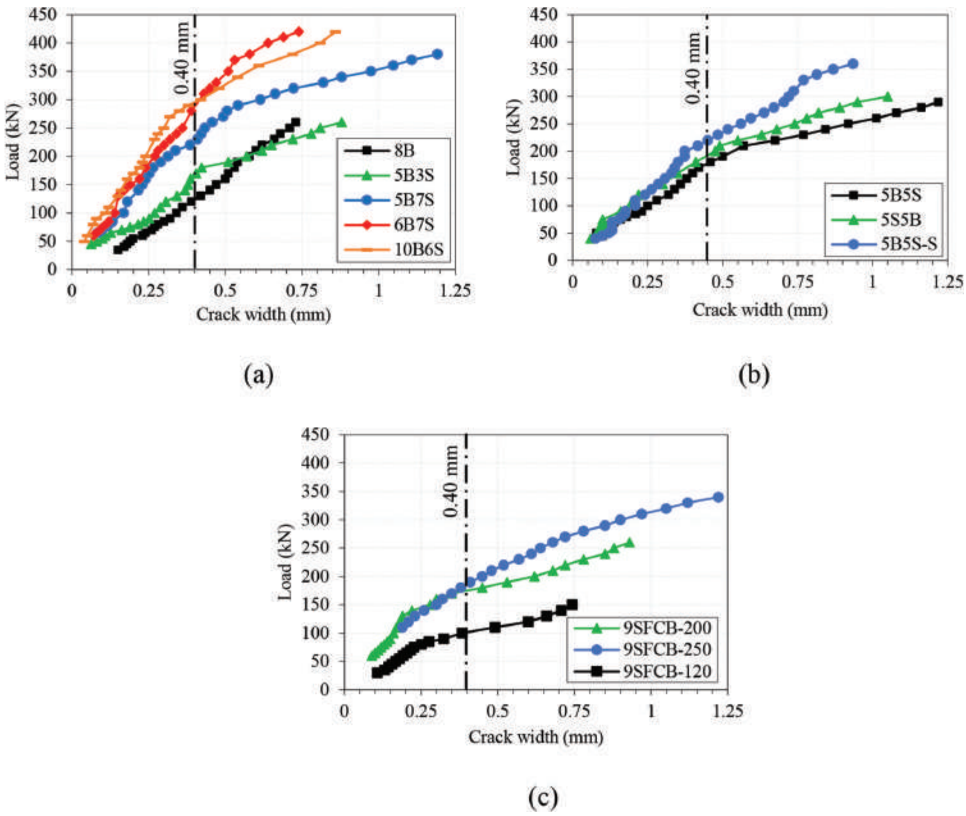

Fig. 9—Load-maximum crack width relationships of tested slabs: (a) Groups A and B; (b) Group C; and (c) Group D. (Note: 1 kN = 0.225 kip; 1 mm = 0.0394 in.)

axial stiffness restricts the propagation of cracks, leading to narrower and shorter cracks. While the overall performance factor retracted slowly with the increase in A_f/A_s, it can record its maximum value at a low value of A_f/A_s. This is because the ultimate deflection and the ultimate load show variations, changing trends with the increase in A_f/A_s. With respect to the reinforcement arrangement, it can be found that the overall performance factor of the single-layer hybrid RC slab 5B5S-S is 6.5, which is larger than that of the double-layer hybrid RC slab (5.7 for 5B5S). The values of the modified overall performance factor satisfied the CSA S6:19 requirements, which ranged from 4.2 to 7.5. The higher values of the overall performance factor imply more ample warning by exhibiting a significant deformation at the ultimate state of the hybrid RC deck slabs before failure. Therefore, the hybrid RC slabs can meet the requirements of deformability by using an adequate value of A_f/A_s.

Crack width

Figure 9 shows the applied load-crack width curves. The load-crack width relationship was almost linear for the pure BFRP-RC slab; however, all hybrid deck slabs exhibited a bilinear curve owing to the yielding of steel bars. In Group A, replacing the BFRP bars with steel bars could restrain crack depth and fast propagation due to the higher elastic modulus of the steel bars. As shown in Fig. 9(a), the crack widths were inversely proportional to the reinforcement ratio. Thus, the measured crack width was lower in the case of Slab 6B7S than in Slab 5B3S. Moreover, a higher ratio of FRP-to-steel amount A_f/A_s led to better secondary stiffness and hence narrower crack widths. Placing BFRP reinforcement in the outer layer recorded a wider crack width for Slab 5B5S, followed by Slabs 5S5B and 5B5S-S. Figure 9(c) shows that higher crack width values were recorded for Slab 9SFCB-120, indicating that decreasing the slab thickness to 120 mm, which is less than the CSA S6:19 minimum allowable thickness of 175 mm, resulted in wider cracks.

Different codes and design guidelines proposed a limit for the crack width of bridge-deck slabs. The American Association of State Highway and Transportation Officials (AASHTO) LRFD Bridge Design Specifications (AASHTO 2018) recommended a limit value of 0.5 mm for maximum crack width when using GFRP reinforcement. Furthermore, CSA S6:19, Clause 16.8.2.3, states that crack width should not exceed 0.5 mm and 0.7 mm for exterior and interior exposure, respectively. As shown in Fig. 9, the maximum crack widths for all test slabs reached 0.4 mm after nearly 54 to 79% of the ultimate load. These loads were much higher than the service loads; thus, the authors recommended that for hybrid RC deck slabs, the maximum crack width limit should be 0.4 mm for exterior exposure.

Reinforcement and concrete strains

The applied load versus measured strains at the midspan of both concretes at the top fiber, and the tensile BFRP or SFCB bars are shown in Fig. 10. Before cracking, all the tested deck slabs showed approximately similar concrete and reinforcement strains. After cracking, the BFRP strain of Slab 8B showed a rapid linear increase, increasing the load up to failure. Using steel bars instead of BFRP bars, Slab 5B3S yielded a significant reduction in BFRP strain compared to Slab 8B, as shown in Fig. 10(a). The influence

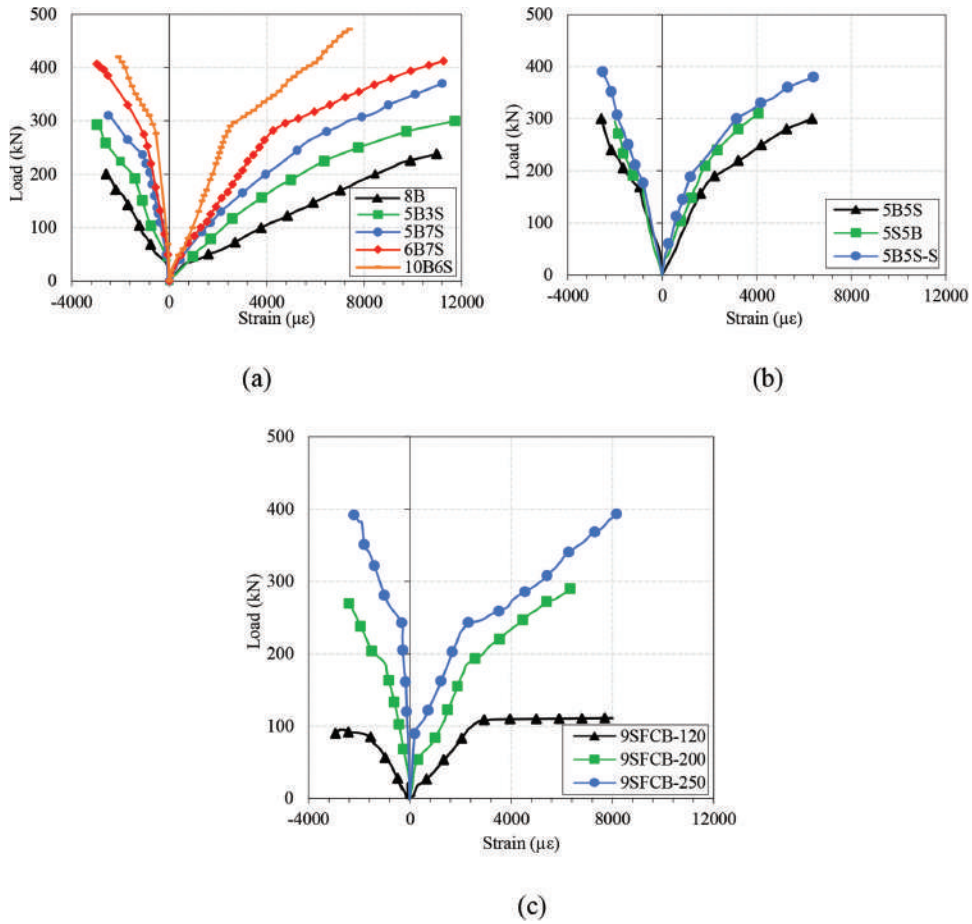

Fig. 10—Load-BFRP reinforcement and concrete-strain relationships: (a) Groups A and B; (b) Group C; and (c) Group D. (Note: 1 kN = 0.225 kip.)

of the reinforcement ratio can be realized in Slabs 5B3S and 10B6S; high reinforcement and lower strains were recorded at the same load levels. Increasing the steel reinforcement controlled the BFRP bar strain development in the hybrid deck slabs, as demonstrated by the lower tensile strain readings in the BFRP bars of Slab 5B3S compared to Slab 5B7S. These results tend to indicate the effect of increasing the effective reinforcement ratio to improve the serviceability performance of the hybrid slabs. Moreover, as the A_f/A_s increased, the BFRP strains decreased, as shown in Fig. 10(a). The BFRP strain in Slab 10B6S (A_f/A_s = 1.58) recorded 2422 με, which was considerably lower than the BFRP strain of Slab 6B7S (A_f/A_s = 0.81) of 4273 με at the yielding load. The secondary stiffness (provided by either BFRP bars or the outer FRP of SFCBs) can restrict the strain development of tensile reinforcements after the steel is yielded (Yang et al. 2020). As shown in Fig. 10(b), there was no clear effect of the reinforcement arrangement on the yielding load, while Slab 5B5S read a high value of BFRP strain of 1932 με, followed by values of 1518 με and 1198 με for Slabs 5S5B and 5B5S-S, respectively. Therefore, the BFRP reinforcement undergoes more tensile stress when placed in the outer layer.

COMPARISON OF TEST RESULTS WITH DIFFERENT DESIGN CODE PREDICTIONS

Prediction of midspan deflection

Equations from different design codes and available models in the literature (refer to the Appendix) were used to predict the midspan deflections of the tested slabs at two load levels, 30 and 60% of the ultimate load capacity, P_u, of each slab. Figure 11 compares the experimental and predicted deflections up to 60% of the ultimate load. Figure 11(a) shows clearly that both the Bischoff model (Bischoff 2007) and ACI 440.1R-15 yielded highly underestimated deflections for Slab 8B; however, CSA S806-12 showed good results with experimental deflections. As shown in Fig. 11(b), the midspan deflections of Slab 5B3S reinforced with a low reinforcement ratio (ρ_{eff} = 0.59%) were underestimated by all the equations; however, the CSA S806-12 equation showed good results with experimental deflections. However, better prediction of deflections was noticed when increasing the reinforcement ratio in Group B. Moreover, a similar trend is also valid for the hybrid slabs of Group C. An excellent agreement between the predicted and the experimental deflections was noticed for Slabs 6B7S and 5B5S, especially for CSA S806-12, illustrated in Fig. 11(e). From a design point of view, CSA S806-12 showed the most accurate method of predicting the deflection of hybrid RC members among all current models at both $0.30P_u$ and $0.60P_u$, with an average of $V_{c,exp}/V_{c,pred}$ of 1.02 ±

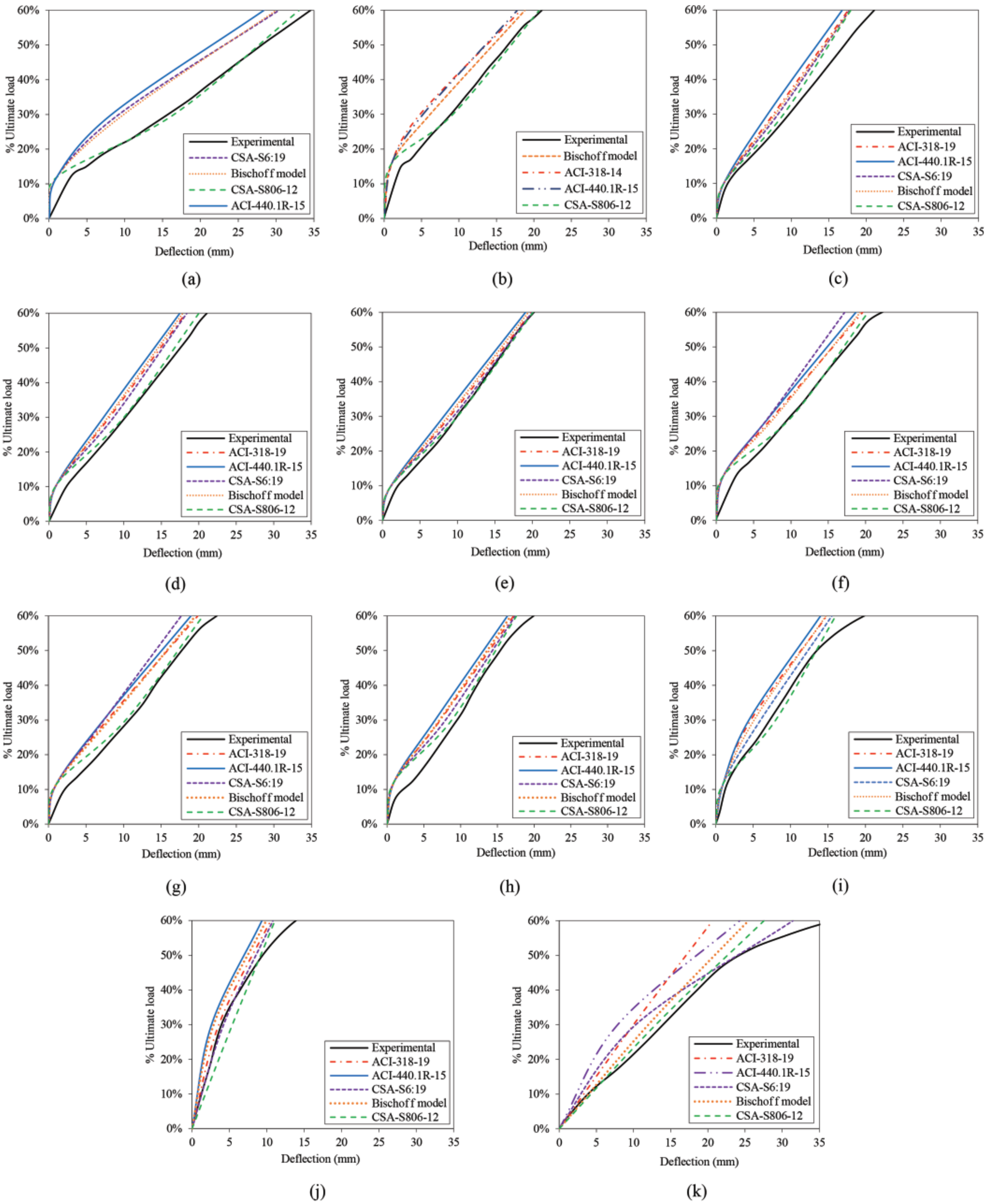

Fig. 11—Comparisons of midspan deflection versus experimental and calculated results of tested deck slabs: (a) 8B; (b) 5B3S; (c) 5B7S; (d) 6B7S; (e) 10B6S; (f) 5B5S; (g) 5S5B; (h) 5B5S-S; (i) 9SFCB-200; (j) 9SFCB-250; and (k) 9SFCB-120. (Note: 1 mm = 0.0394 in.)

0.26 and 1.12 ± 0.10. This might be caused by the cracked moment of inertia in the closed-form equation suggested by CSA S806-12.

Bond-dependent coefficient prediction

Both design codes ACI CODE-440.11-22 (ACI Committee 440 2022) and CSA S6:19 provided the same expression for predicting the maximum crack width of FRP-RC members, as shown in Eq. (9). The bond-dependent coefficient, k_b, considered the variety of concrete sections and different FRP bars. In addition, the bond degree of FRP bars within the concrete, which is always indicated by the bond coefficient in existing design codes, should be determined before computing the crack width. The determination of the bond coefficient, k_b, is suggested to be realized by substituting the experimentally obtained crack widths and tensile strains of the longitudinal reinforcements into Eq. (9). It should be noted that w in Eq. (9) denotes the maximum crack width at the bottom of the tension face, while the measured crack widths of the present study were at the level of BFRP reinforcement. Therefore, the amplification factor β in Eq. (9), which transfers the crack width at the level of reinforcements to that of the tension face, was not considered.

$$w = 2\varepsilon_f \beta k_b \sqrt{{d_c}^2 + \left(\frac{s}{2}\right)^2} \tag{9a}$$

$$\varepsilon_f = \frac{M_a}{(E_f A_f + E_s A_s)\left[1 - \left(\frac{k}{3}\right)\right]d} \tag{9b}$$

$$\beta = \frac{h - kd}{d - kd} \tag{9c}$$

Herein, the slab results were used to assess the value of the bond coefficient of BFRP bars, k_b, with Eq. (9). The k_b was calculated at two load levels: at $0.3P_u$, which is considered the service load level (Mota et al. 2006; Bischoff et al. 2009; El-Nemr et al. 2013), and at $0.67P_u$, in which the crack pattern reached a stabilized state and no new cracks appeared. Table 5 reports the average k_b measured for each slab specimen. The results showed some variations between k_b determined at the different load levels. The average k_b value was 1.27 ± 0.14 with a coefficient of variation (COV) of 11% for BFRP bars with ribbed surfaces. It was found that this value is close to that recommended by Shield et al. (2019) and ACI CODE-440.11-22 of 1.2 for GFRP bars. However, CSA S6:19 proposed using a k_b of 1.0 for ribbed FRP bars; thus, CSA S6:19 is nonconservative.

Table 5—Bond-dependent coefficient, k_b

Slab	k_b		
	$0.30P_u$	$0.67P_u$	Average
8B	1.11	1.07	1.09
5B3S	1.38	1.37	1.38
5B7S	1.22	1.42	1.32
6B7S	0.92	1.45	1.19
10B6S	1.32	0.97	1.15
5B5S	1.42	1.44	1.43
5S5B	1.43	1.41	1.42
5B5S-S	0.97	1.25	1.11
9SFCB-200	1.28	1.42	1.35
9SFCB-250	1.03	1.12	1.08
9SFCB-120	1.46	1.38	1.42
Average			1.27
Standard deviation			0.14
Coefficient of variation, %			11

Prediction of shear strength

The shear capacities of hybrid reinforced slabs were predicted with the shear models provided in different design codes. To date, no design code or guidelines have been published for designing concrete structures with hybrid reinforcement. Therefore, the authors suggested a modification for some equations that consider the effect of hybrid reinforcement. For example, for the AASHTO specifications (AASHTO 2018), it is recommended to account for the ratio between the stiffness of longitudinal steel reinforcement, E_s, to that of FRP reinforcement, E_f. For CSA S806-12, which considers the effect of FRP reinforcement, ρ_f, the authors proposed replacing the FRP reinforcement with the mechanical reinforcing index, $\rho_{f,eq}$, as shown in Eq. (10). However, CSA S6:19 considers FRP axial stiffness in the shear equations; thus, the authors suggested accounting for the axial stiffness of both steel and FRP reinforcement rather than only FRP reinforcement, as shown in Eq. (11). Moreover, ACI CODE-440.11-22 indirectly incorporates both steel and FRP reinforcement through the coefficient k. Table 6 (refer to the Appendix) summarizes all shear equations after introducing the modifications.

$$\rho_{f,eq} = \rho_f + \frac{f_y}{f_{fu}}\rho_s \tag{10}$$

$$EA = E_s A_s + E_f A_f \tag{11}$$

The accuracy of the predicted results was evaluated and discussed by comparing their predictions with the values that were experimentally determined from the tested slabs. The experimental-to-predicted shear ratios, $V_{c,exp}/V_{c,pred}$, are presented in Table 7. From the results of the prediction, AASHTO yielded very good agreement with the experimental results, with an average $V_{c,exp}/V_{c,pred}$ of 1.23 ± 0.36. After introducing the modifications, ACI CODE-440.11-22 and CSA S806-12 yielded good yet conservative predictions with average $V_{c,exp}/V_{c,pred}$ of 1.65 ± 0.21 and 1.59 ± 0.33 and a COV of 13 and 21%, respectively. However, CSA S6:19 showed very conservative predictions with an average $V_{c,exp}/V_{c,pred}$ of 2.01 ± 0.30 compared to AASHTO. This might be attributed to CSA S6:19 accounting for the effect of the longitudinal FRP reinforcement ratio and the elastic modulus in one term (axial stiffness, EA) rather than the other codes calculating them separately. Generally, the modifications in the shear equations proposed in this study are suitable for the predictions of the shear capacities of hybrid RC members reinforced with steel and BFRP bars, while extensive investigations are needed in the future to confirm these modifications.

Table 6—Modified shear equations for hybrid RC members

Reference	Equation
ACI CODE-440.11-22	$V_c = 0.4\sqrt{f_c'}b_w kd$
AASHTO (2018)	$V_c = 0.16\sqrt{f_c'}b_w c(E_s/E_f)$; $c = kd$
CSA S806-12	$V_{c,mod} = 0.11\phi_c\sqrt{f_c'}b_w d_v \leq 0.05\lambda\phi_c k_m k_{r,mod}(f_c')^{1/3}b_w d_v \leq 0.22\phi_c\sqrt{f_c'}b_w d_v$ $k_m = \sqrt{\frac{V_u d}{M_u}} \leq 1.0$; $k_{r,mod} = 1 + (E_f\rho_{sf,f})^{1/3}$
CSA S6:19	$V_c = 2.5\beta\phi_c f_{cr} b_w d_v$ $\beta_{mod} = \left[\frac{0.4}{1 + 1500\varepsilon_{x,mod}}\right]\left[\frac{1300}{1000 + s_{ze}}\right]$ $\varepsilon_{x,mod} = \frac{\frac{M_u}{d_v} + V_u}{2(E_f A_f + E_s A_s)} \leq 0.003$; $s_{ze} = \frac{35 s_z}{15 + a_g} \leq 0.85 s_z$

Table 7—Experimental-to-predicted shear capacity

Slab	V_u	$V_u/V_{u,pred}$			
		ACI CODE-440.11-22	AASHTO (2018)	CSA S806-12	CSA S6:19
8B	147.5	2.06	2.06	1.24	1.83
5B3S	157	1.49	1.48	1.31	1.77
6B7S	218.5	1.70	1.07	2.01	2.24
10B6S	235	1.86	1.17	2.19	2.46
5B5S	162.5	1.45	0.91	1.51	1.71
5S5B	167.5	1.55	0.98	1.55	1.79
5B5S-S	198	1.71	1.17	1.67	2.44
9SFCB-200	146	1.41	0.97	1.24	1.83
Average		1.65	1.23	1.59	2.01
Standard deviation		0.21	0.36	0.33	0.30
Coefficient of variation, %		13	29	21	15

Note: $V_{c,exp}$ is factored shear (kN); 1 kN = 0.225 kip.

DESIGN RECOMMENDATIONS FOR HYBRID RC MEMBERS WITHOUT SHEAR REINFORCEMENT

Based on the experimental results in this study, under-reinforced hybrid RC slabs exhibit higher stiffness and strength with ductile behavior before failure compared to FRP-RC slabs, which is still adequate to achieve the safety requirement. Hence, it is recommended that designers should follow the under-reinforced section procedures when using hybrid (FRP and steel) bars as tensile reinforcement. Moreover, it is necessary that engineers should be aware of the FRP-to-steel ratio, A_f/A_s, when designing such sections. It is suggested to use a high A_f/A_s, which means a large amount of FRP bars to provide high strength and avoid excessive deflection and rupture of FRP bars after the steel yields. In contrast, using a low A_f/A_s can ensure the ductile performance guaranteed by the yielding of steel bars. In addition, using the proposed shear equations presented in this study can assure the ductile failure of RC flexural elements by making the shear capacity at all sections equal to or greater than the flexural one. Recently, some design recommendations were proposed through an experimental and numerical study made by the authors (Ali et al. 2023). However, further research on the concrete contribution to the shear strength of hybrid RC members is needed.

SUMMARY AND CONCLUSIONS

Eleven deck slabs were constructed and tested up to failure to study the mechanical behavior of hybrid deck slabs. The test parameters are reinforcement type, ratio, and arrangement; the fiber-reinforced polymer (FRP)-to-steel ratio A_f/A_s; and slab thickness. Based on the results and discussion presented herein, the following conclusions are obtained:

1. The observed failure mode of the basalt FRP (BFRP)-reinforced concrete (RC) slab was an undesirable brittle shear failure, while hybrid RC slabs showed gradual shear-compression failure, flexural-shear failure, and flexural failure. The failure of the hybrid RC slabs is significantly affected by the effective reinforcement ratio and A_f/A_s; it becomes more severe when increasing the reinforcement ratio with a high value of A_f/A_s.

2. The effective reinforcement ratio and A_f/A_s had considerable influence on the post-cracking stiffness of the hybrid deck slabs. In addition, increasing the reinforcement ratio by 100% increased the ultimate capacity by 50%. Increasing A_f/A_s from 0.68 to 1.58 significantly reduced the midspan deflections and crack widths and increased the ultimate capacity by 14%.

3. The existing models for predicting the midspan deflections are conservative in predicting the deflections of hybrid RC slabs. However, the models give good predictions for slabs that have high effective reinforcement ratios. CSA

S806-12 provided accurate predictions with the experimental results.

4. The test results were used to assess the bond-dependent coefficient of BFRP bars. The calculations yielded an average bond-dependent coefficient, k_b, of 1.27, close to the 1.2 recommended by ACI CODE-440.11-22 and larger than the 1.0 proposed by CSA S6:19.

5. The proposed modifications to the design code equations were verified to accurately predict the shear capacity of hybrid RC slabs without shear reinforcement. The AASHTO equation provided the most accurate shear capacity prediction for hybrid RC slabs, with an average ratio of $V_{c,exp}/V_{c,pred}$ of 1.23.

AUTHOR BIOS

ACI member **Yahia M. S. Ali** *is a PhD Candidate in the School of Civil Engineering at Southeast University, Nanjing, Jiangsu, China, and a Teaching Assistant in the Department of Civil Engineering at Assiut University, Assiut, Egypt. He received his BS and MSc in structural engineering from Assiut University. His research interests include structural design and the analysis and testing of concrete structures reinforced with fiber-reinforced polymers (FRPs).*

Xin Wang *is a Professor in the Key Laboratory of Concrete and Prestressed Concrete Structures of Ministry of Education at Southeast University, and a Professor in the Department of Civil Engineering at Southeast University. He received his BS and MSc from Southeast University in 2002 and 2006, respectively, and his PhD from Ibaraki University, Mito, Ibaraki, Japan, in 2010. His research interests include FRP composites and concrete structures with FRP composites.*

Shui Liu *is a PhD Candidate in the Key Laboratory of Concrete and Prestressed Concrete Structures of Ministry of Education at Southeast University and in the Department of Civil Engineering at Southeast University. His research interests include the analysis and design of concrete structures reinforced with a combination of FRP and steel bars.*

Zhishen Wu *is a Professor in the School of Civil Engineering at Southeast University. He received his BS and MS from Southeast University, and his PhD from Nagoya University, Nagoya, Aichi, Japan. His research interests include FRP composites and technologies, maintenance and life-cycle engineering, failure mechanics of composite materials, and structural health monitoring infrastructure systems.*

ACKNOWLEDGMENTS

The authors gratefully acknowledge the financial support provided by the National Key Research and Development Program of China (No. 2022YFB3706503) and the National Natural Science Foundation of China (Grant 52278244).

NOTATION

A_f = area of BFRP reinforcement
A_s = area of steel reinforcement
a = distance between support and point load (shear span)
a_g = nominal maximum size of coarse aggregate
b_w = width of cross section
c = distance from extreme fiber in compression to neutral axis
d = distance from extreme fiber in compression to center of tensile reinforcement
d_f = distance from extreme compression fiber to center of FRP bars
d_s = distance from extreme compression fiber to center of steel bars
d_v = effective shear depth
E_c = modulus of elasticity of concrete
E_f = modulus of elasticity of BFRP bars
E_I = elastic modulus
E_{II} = post-elastic modulus
E_s = modulus of elasticity of steel bars
f_c' = concrete compressive strength
f_{cr} = cracking strength
f_{cu} = cube compressive strength
f_{fu} = ultimate tensile stress in BFRP bars
f_y = yield stress in steel reinforcement
h = overall member thickness
I_{cr} = cracked moment of inertia
I_e = effective moment of inertia
I_g = gross moment of inertia
J = overall performance factor
J_{mod} = modified overall performance factor
k_b = bond coefficient
k_m = moment-shear interaction factor
$k_{r,mod}$ = reinforcement stiffness factor
L = slab length
L_g = distance from support to point where $M = M_{cr}$
M_a = applied moment at critical section
M_{cr} = cracking moment
M_{exp} = experimental moment capacity
M_{pred} = predicted moment capacity
M_s = service moment
M_u = ultimate moment
M_y = yielding moment
n_f = ratio of modulus of elasticity of BFRP bars to modulus of elasticity of concrete
n_s = ratio of modulus of elasticity of steel bars to modulus of elasticity of concrete
P_{cr} = cracking load
P_{th} = theoretical flexural capacity
P_u = ultimate load
P_y = yielding load
s = spacing of reinforcing bars
s_{ze} = effective crack spacing for members without stirrups
$V_{c,mod}$ = modified one-way shear strength provided by concrete and flexural reinforcement
V_u = factored shear
w = maximum crack width
α_1 = ratio of average stress of equivalent rectangular stress block to cylinder compressive strength of concrete
β = ratio of distance between neutral axis and tension face to distance between neutral axis and centroid of reinforcement
β_1 = ratio of depth of equivalent rectangular stress block to depth of neutral axis
Δ_{cr} = cracking deflection at midspan of slab
Δ_m = maximum deflection at midspan of the slab
Δ_u = ultimate deflection at midspan of slab
Δ_y = yielding deflection at midspan of slab
ε_{cu} = maximum concrete compressive strain (0.003 for ACI 318-19 [ACI Committee 318 2019] provisions)
ε_f = tensile strain in BFRP bars
ε_s = yield strain in steel bars
$\varepsilon_{x,mod}$ = modified longitudinal strain at middepth of cross section
ϕ_c = material reduction factor for concrete (taken as unity in this paper)
η = reduction coefficient
λ = concrete density factor
ρ_f = BFRP reinforcement ratio
$\rho_{f,b}$ = FRP balanced reinforcement ratio
$\rho_{f,eq}$ = mechanical reinforcing index
ρ_s = steel reinforcement ratio
$\rho_{s,b}$ = steel balanced reinforcement ratio
$\rho_{sf,f}$ = effective reinforcement ratio in hybrid sections with respect to FRP
$\rho_{sf,s}$ = effective reinforcement ratio in hybrid sections with respect to steel
Ψ_s = curvature at service moment
Ψ_u = curvature at ultimate moment
Ψ_y = curvature at yield moment

REFERENCES

AASHTO, 2018, "AASHTO LRFD Bridge Design Guide Specifications for GFRP-Reinforced Concrete," second edition, American Association of State Highway and Transportation Officials, Washington, DC.

Abdul-Salam, B.; Farghaly, A. S.; and Benmokrane, B., 2016, "Mechanisms of Shear Resistance of One-Way Concrete Slabs Reinforced with FRP Bars," *Construction and Building Materials*, V. 127, Nov., pp. 959-970. doi: 10.1016/j.conbuildmat.2016.10.015

ACI Committee 318, 2019, "Building Code Requirements for Structural Concrete (ACI 318-19) and Commentary (ACI 318R-19) (Reapproved 2022)," American Concrete Institute, Farmington Hills, MI, 624 pp.

ACI Committee 440, 2015, "Guide for the Design and Construction of Structural Concrete Reinforced with Fiber-Reinforced Polymer (FRP) Bars (ACI 440.1R-15)," American Concrete Institute, Farmington Hills, MI, 88 pp.

ACI Committee 440, 2022, "Building Code Requirements for Structural Concrete Reinforced with Glass Fiber-Reinforced Polymer (GFRP) Bars—Code and Commentary (ACI CODE-440.11-22)," American Concrete Institute, Farmington Hills, MI, 260 pp.

Aiello, M. A., and Ombres, L., 2002, "Structural Performances of Concrete Beams with Hybrid (Fiber-Reinforced Polymer-Steel) Reinforcements," *Journal of Composites for Construction*, ASCE, V. 6, No. 2, May, pp. 133-140. doi: 10.1061/(ASCE)1090-0268(2002)6:2(133)

Ali, Y. M. S.; Wang, X.; Ding, L.; Liu, S.; and Wu, Z., 2023, "Experimental and Numerical Investigations of the Effects of Various Tensile Reinforcement Types on the Structural Behavior of Concrete Bridge Deck Slabs," *Engineering Structures*, V. 285, June, Article No. 116036. doi: 10.1016/j.engstruct.2023.116036

ASTM D7205/D7205M-06(2016), 2016, "Standard Test Method for Tensile Properties of Fiber Reinforced Polymer Matrix Composite Bars," ASTM International, West Conshohocken, PA, 13 pp.

Bischoff, P. H., 2007, "Deflection Calculation of FRP Reinforced Concrete Beams Based on Modifications to the Existing Branson Equation," *Journal of Composites for Construction*, ASCE, V. 11, No. 1, Feb., pp. 4-14. doi: 10.1061/(ASCE)1090-0268(2007)11:1(4)

Bischoff, P. H.; Gross, S.; and Ospina, C. E., 2009, "The Story Behind Proposed Changes to ACI 440 Deflection Requirements for FRP-Reinforced Concrete," *Serviceability of Concrete Members Reinforced with Internal/External FRP Reinforcement*, SP-264, C. Ospina, P. Bischoff, and T. Alkhrdaji, eds., American Concrete Institute, Farmington Hills, MI, pp. 53-76.

CSA S6:19, 2019, "Canadian Highway Bridge Design Code," CSA Group, Toronto, ON, Canada, 1182 pp.

CSA S806-12 (R2017), 2017, "Design and Construction of Building Structures with Fibre-Reinforced Polymers," CSA Group, Toronto, ON, Canada.

Duic, J.; Kenno, S.; and Das, S., 2018, "Performance of Concrete Beams Reinforced with Basalt Fibre Composite Rebar," *Construction and Building Materials*, V. 176, July, pp. 470-481. doi: 10.1016/j.conbuildmat.2018.04.208

El-Nemr, A.; Ahmed, E. A.; and Benmokrane, B., 2013, "Flexural Behavior and Serviceability of Normal- and High-Strength Concrete Beams Reinforced with Glass Fiber-Reinforced Polymer Bars," *ACI Structural Journal*, V. 110, No. 6, Nov.-Dec., pp. 1077-1088.

El-Salakawy, E., and Benmokrane, B., 2004, "Serviceability of Concrete Bridge Deck Slabs Reinforced with Fiber-Reinforced Polymer Composite Bars," *ACI Structural Journal*, V. 101, No. 5, Sept.-Oct., pp. 727-736.

El-Salakawy, E. F.; Kassem, C.; and Benmokrane, B., 2003, "Flexural Behaviour of Bridge Deck Slabs Reinforced with FRP Composite Bars," *Fibre-Reinforced Polymer Reinforcement for Concrete Structures: Proceedings of the Sixth International Symposium on FRP Reinforcement for Concrete Structures (FRPRCS-6)*, K. H. Tan, ed., World Scientific Publishing, Singapore, pp. 1291-1300.

El-Sayed, A.; El-Salakawy, E.; and Benmokrane, B., 2005, "Shear Strength of One-Way Concrete Slabs Reinforced with Fiber-Reinforced Polymer Composite Bars," *Journal of Composites for Construction*, ASCE, V. 9, No. 2, Apr., pp. 147-157. doi: 10.1061/(ASCE)1090-0268(2005)9:2(147)

El-Sayed, A. K.; El-Salakawy, E. F.; and Benmokrane, B., 2006a, "Shear Strength of FRP-Reinforced Concrete Beams without Transverse Reinforcement," *ACI Structural Journal*, V. 103, No. 2, Mar.-Apr., pp. 235-243.

El-Sayed, A. K.; El-Salakawy, E. F.; and Benmokrane, B., 2006b, "Shear Capacity of High-Strength Concrete Beams Reinforced with FRP Bars," *ACI Structural Journal*, V. 103, No. 3, May-June, pp. 383-389.

El Refai, A.; Abed, F.; and Al-Rahmani, A., 2015, "Structural Performance and Serviceability of Concrete Beams Reinforced with Hybrid (GFRP and Steel) Bars," *Construction and Building Materials*, V. 96, Oct., pp. 518-529. doi: 10.1016/j.conbuildmat.2015.08.063

Elgabbas, F.; Ahmed, E. A.; and Benmokrane, B., 2016, "Experimental Testing of Concrete Bridge-Deck Slabs Reinforced with Basalt-FRP Reinforcing Bars under Concentrated Loads," *Journal of Bridge Engineering*, ASCE, V. 21, No. 7, July, p. 04016029. doi: 10.1061/(ASCE)BE.1943-5592.0000892

Ferrier, E.; Michel, L.; Zuber, B.; and Chanvillard, G., 2015, "Mechanical Behaviour of Ultra-High-Performance Short-Fibre-Reinforced Concrete Beams with Internal Fibre Reinforced Polymer Bars," *Composites Part B: Engineering*, V. 68, Jan., pp. 246-258. doi: 10.1016/j.compositesb.2014.08.001

Ge, W.; Wang, Y.; Ashour, A.; Lu, W.; and Cao, D., 2020, "Flexural Performance of Concrete Beams Reinforced with Steel–FRP Composite Bars," *Archives of Civil and Mechanical Engineering*, V. 20, No. 2, June, Article No. 56. doi: 10.1007/s43452-020-00058-6

Ge, W.; Zhang, J.; Cao, D.; and Tu, Y., 2015, "Flexural Behaviors of Hybrid Concrete Beams Reinforced with BFRP Bars and Steel Bars," *Construction and Building Materials*, V. 87, July, pp. 28-37. doi: 10.1016/j.conbuildmat.2015.03.113

Goldston, M.; Remennikov, A.; and Sheikh, M. N., 2016, "Experimental Investigation of the Behaviour of Concrete Beams Reinforced with GFRP Bars under Static and Impact Loading," *Engineering Structures*, V. 113, Apr., pp. 220-232. doi: 10.1016/j.engstruct.2016.01.044

Ibrahim, A. I.; Wu, G.; and Sun, Z.-Y., 2017, "Experimental Study of Cyclic Behavior of Concrete Bridge Columns Reinforced by Steel Basalt-Fiber Composite Bars and Hybrid Stirrups," *Journal of Composites for Construction*, ASCE, V. 21, No. 2, Apr., p. 04016091. doi: 10.1061/(ASCE)CC.1943-5614.0000742

Liu, S.; Wang, X.; Ali, Y. M. S.; Su, C.; and Wu, Z., 2022, "Flexural Behavior and Design of Under-Reinforced Concrete Beams with BFRP and Steel Bars," *Engineering Structures*, V. 263, July, Article No. 114386. doi: 10.1016/j.engstruct.2022.114386

Matta, F.; El-Sayed, A. K.; Nanni, A.; and Benmokrane, B., 2013, "Size Effect on Concrete Shear Strength in Beams Reinforced with Fiber-Reinforced Polymer Bars," *ACI Structural Journal*, V. 110, No. 4, July-Aug., pp. 617-628.

Michaluk, C. R.; Rizkalla, S. H.; Tadros, G.; and Benmokrane, B., 1998, "Flexural Behavior of One-Way Concrete Slabs Reinforced by Fiber Reinforced Plastic Reinforcements," *ACI Structural Journal*, V. 95, No. 3, May-June, pp. 353-364.

Mota, C.; Alminar, S.; and Svecova, D., 2006, "Critical Review of Deflection Formulas for FRP-RC Members," *Journal of Composites for Construction*, ASCE, V. 10, No. 3, June, pp. 183-194. doi: 10.1061/(ASCE)1090-0268(2006)10:3(183)

Nanni, A.; Henneke, M. J.; and Okamoto, T., 1994, "Tensile Properties of Hybrid Rods for Concrete Reinforcement," *Construction and Building Materials*, V. 8, No. 1, pp. 27-34. doi: 10.1016/0950-0618(94)90005-1

Nguyen, P. D.; Dang, V. H.; and Vu, N. A., 2020, "Performance of Concrete Beams Reinforced with Various Ratios of Hybrid GFRP/Steel Bars," *Civil Engineering Journal*, V. 6, No. 9, pp. 1652-1669. doi: 10.28991/cej-2020-03091572

Pang, L.; Qu, W.; Zhu, P.; and Xu, J., 2016, "Design Propositions for Hybrid FRP-Steel Reinforced Concrete Beams," *Journal of Composites for Construction*, ASCE, V. 20, No. 4, Aug., p. 04015086. doi: 10.1061/(ASCE)CC.1943-5614.0000654

Qin, R.; Zhou, A.; and Lau, D., 2017, "Effect of Reinforcement Ratio on the Flexural Performance of Hybrid FRP Reinforced Concrete Beams," *Composites Part B: Engineering*, V. 108, Jan., pp. 200-209. doi: 10.1016/j.compositesb.2016.09.054

Qu, W.; Zhang, X.; and Huang, H., 2009, "Flexural Behavior of Concrete Beams Reinforced with Hybrid (GFRP and Steel) Bars," *Journal of Composites for Construction*, ASCE, V. 13, No. 5, Oct., pp. 350-359. doi: 10.1061/(ASCE)CC.1943-5614.0000035

Ruan, X.; Lu, C.; Xu, K.; Xuan, G.; and Ni, M., 2020, "Flexural Behavior and Serviceability of Concrete Beams Hybrid-Reinforced with GFRP Bars and Steel Bars," *Composite Structures*, V. 235, Mar., Article No. 111772. doi: 10.1016/j.compstruct.2019.111772

Safan, M. A., 2013, "Flexural Behavior and Design of Steel-GFRP Reinforced Concrete Beams," *ACI Materials Journal*, V. 110, No. 6, Nov.-Dec., pp. 677-686.

Shield, C.; Brown, V.; Bakis, C. E.; and Gross, S., 2019, "A Recalibration of the Crack Width Bond-Dependent Coefficient for GFRP-Reinforced Concrete," *Journal of Composites for Construction*, ASCE, V. 23, No. 4, Aug., p. 04019020. doi: 10.1061/(ASCE)CC.1943-5614.0000978

Sun, Z.; Fu, L.; Feng, D.-C.; Vatuloka, A. R.; Wei, Y.; and Wu, G., 2019, "Experimental Study on the Flexural Behavior of Concrete Beams Reinforced with Bundled Hybrid Steel/FRP Bars," *Engineering Structures*, V. 197, Oct., Article No. 109443. doi: 10.1016/j.engstruct.2019.109443

Sun, Z.-Y.; Wu, G.; Wu, Z.-S.; and Zhang, M., 2011, "Seismic Behavior of Concrete Columns Reinforced by Steel-FRP Composite Bars," *Journal of Composites for Construction*, ASCE, V. 15, No. 5, Oct., pp. 696-706. doi: 10.1061/(ASCE)CC.1943-5614.0000199

Sun, Z. Y.; Yang, Y.; Qin, W. H.; Ren, S. T.; and Wu, G., 2012, "Experimental Study on Flexural Behavior of Concrete Beams Reinforced by Steel-Fiber Reinforced Polymer Composite Bars," *Journal of Reinforced Plastics and Composites*, V. 31, No. 24, Dec., pp. 1737-1745. doi: 10.1177/0731684412456446

Tureyen, A. K., and Frosch, R. J., 2002, "Shear Tests of FRP-Reinforced Concrete Beams without Stirrups," *ACI Structural Journal*, V. 99, No. 4, July-Aug., pp. 427-434.

Wang, X.; Liu, S.; Shi, Y.; Wu, Z.; and He, W., 2022, "Integrated High-Performance Concrete Beams Reinforced with Hybrid BFRP and Steel Bars," *Journal of Structural Engineering*, ASCE, V. 148, No. 1, Jan., p. 04021235. doi: 10.1061/(ASCE)ST.1943-541X.0003207

Wu, G.; Dong, Z.-Q.; Wang, X.; Zhu, Y.; and Wu, Z.-S., 2015, "Prediction of Long-Term Performance and Durability of BFRP Bars under the

Combined Effect of Sustained Load and Corrosive Solutions," *Journal of Composites for Construction*, ASCE, V. 19, No. 3, June, pp. 1-9. doi: 10.1061/(ASCE)CC.1943-5614.0000517

Wu, G.; Sun, Z. Y.; Wu, Z. S.; and Luo, Y. B., 2012, "Mechanical Properties of Steel-FRP Composite Bars (SFCBs) and Performance of SFCB Reinforced Concrete Structures," *Advances in Structural Engineering*, V. 15, No. 4, Apr., pp. 625-635. doi: 10.1260/1369-4332.15.4.625

Wu, Z.; Fahmy, M. F. M.; and Wu, G., 2009, "Safety Enhancement of Urban Structures with Structural Recoverability and Controllability," *Journal of Earthquake and Tsunami*, V. 3, No. 3, Sept., pp. 143-174. doi: 10.1142/S1793431109000561

Xingyu, G.; Yiqing, D.; and Jiwang, J., 2020, "Flexural Behavior Investigation of Steel-GFRP Hybrid-Reinforced Concrete Beams Based on Experimental and Numerical Methods," *Engineering Structures*, V. 206, Mar., Article No. 110117. doi: 10.1016/j.engstruct.2019.110117

Yang, Y.; Sun, Z.-Y.; Wu, G.; Cao, D.-F.; and Pan, D., 2020, "Experimental Study of Concrete Beams Reinforced with Hybrid Bars (SFCBs and BFRP Bars)," *Materials and Structures*, V. 53, No. 4, Aug., Article No. 77. doi: 10.1617/s11527-020-01514-8

Yinghao, L., and Yong, Y., 2013, "Arrangement of Hybrid Rebars on Flexural Behavior of HSC Beams," *Composites Part B: Engineering*, V. 45, No. 1, Feb., pp. 22-31. doi: 10.1016/j.compositesb.2012.08.023

Yoo, D.-Y.; Banthia, N.; and Yoon, Y.-S., 2016, "Flexural Behavior of Ultra-High-Performance Fiber-Reinforced Concrete Beams Reinforced with GFRP and Steel Rebars," *Engineering Structures*, V. 111, Mar., pp. 246-262. doi: 10.1016/j.engstruct.2015.12.003